PCCP

RSC Publishing

PAPER

View Article Online
View Journal | View Issue

Cite this: *Phys. Chem. Chem. Phys.*, 2013, **15**, 20590

Structure and phase behavior of colloidal dumbbells with tunable attractive interactions

G. Munaò,*[a] D. Costa,[b] A. Giacometti,[c] C. Caccamo[b] and F. Sciortino[a]

Received 11th June 2013,
Accepted 14th October 2013

DOI: 10.1039/c3cp52425f

www.rsc.org/pccp

We investigate thermodynamic and structural properties of colloidal dumbbells in the framework provided by the Reference Interaction Site Model (RISM) theory of molecular fluids and Monte Carlo simulations. We consider two different models: in the first one we set identical square-well attractions on the two tangent spheres constituting the molecule (SW–SW model); in the second scheme, one of the square-well interactions is switched off (HS–SW model). Appreciable differences emerge between the physical properties of the two models. Specifically, the $k \to 0$ behavior of SW–SW structure factors $S(k)$ points to the presence of a gas–liquid coexistence, as confirmed by subsequent fluid phase equilibria calculations. Conversely, the HS–SW $S(k)$ develops a low-k peak, signaling the presence of aggregates; such a process destabilizes the gas–liquid phase separation, promoting at low temperatures the formation of a cluster phase, whose structure depends on the system density. We further investigate such differences by studying the phase behavior of a series of intermediate models, obtained from the original SW–SW by progressively reducing the depth of one square-well interaction. RISM structural predictions positively reproduce the simulation data, including the rise of $S(k \to 0)$ in the SW–SW model and the low-k peak in the HS–SW structure factor. As for the phase behavior, RISM agrees with Monte Carlo simulations in predicting a gas–liquid coexistence for the SW–SW model (though the critical parameters appear overestimated by the theory) and its progressive disappearance when moving toward the HS–SW model.

Introduction

Physical properties of colloidal molecules constitute one of the most interesting and investigated branches of soft matter physics. The recent developments in experimental techniques offer nowadays the possibility to engineer colloidal particles with different sizes, shapes and chemical compositions[1–6] and this opportunity to finely tune the interaction properties of colloidal systems gives rise to rich phase behaviors.[7] Within this large class of molecules, colloidal particles constituted by two interaction sites (dumbbells) have been recently investigated by means of both experimental techniques[8–17] and theoretical and numerical studies.[18–30] In particular, it has been shown that dumbbell colloids can be used as building blocks to fabricate new photonic crystals[14] and other complex structures;[10] furthermore, recent progress in experimental synthesis permits the fabrication of asymmetric functionalized dimer particles on a large scale (see ref. 16 and 17 and references therein). As for simulations and theoretical investigations of colloidal dumbbells, previous studies on the so-called vibrating square-well dumbbells[25,29] have shown a phase behavior strictly dependent on both the aspect ratio and the strength of the square-well interaction, with drastic consequences on the phase diagram. Other recent studies have dealt with the phase behavior of dipolar colloidal gels,[24,28] the dynamical arrest in a liquid of symmetric dumbbells,[22] the dynamics of a glass-forming liquid of dumbbells,[21] the density profiles of confined hard-dumbbell fluids[27] and the two-dimensional structure of dipolar heterogeneous dumbbells.[30] More generally, such particles constitute a useful prototype model for a variety of molecular systems, whose structural and thermodynamic properties are still under scrutiny.

In this article we investigate the structure and phase behavior of model colloidal dumbbells by means of integral equation theories of molecular fluids and Monte Carlo simulations. Specifically, we first consider dumbbells constituted by two identical tangent Hard Spheres (HS) interacting with the sites of another dumbbell by means of a Square-Well (SW) attractive potential (SW–SW model hereafter); such a model, with different SW parameters, has also been analyzed in the past by means of different theoretical techniques.[18,19] We then examine a second model, in which one of

[a] *Dipartimento di Fisica, Università di Roma "La Sapienza", Piazzale Aldo Moro 2, 00185 Roma, Italy. E-mail: gmunao@gmail.com*
[b] *Dipartimento di Fisica e di Scienze della Terra, Universitá degli Studi di Messina, Viale F. Stagno d'Alcontres 31, 98166 Messina, Italy*
[c] *Dipartimento di Scienze Molecolari e Nanosistemi, Universita Ca' Foscari Venezia, Calle Larga S.Marta DD2137, Venezia I-30123, Italy*

the square-well interactions is switched off, so as to leave a bare hard-sphere repulsion on the corresponding site (HS–SW model). The HS–SW model may be seen as an extension to a dumbbell scheme of Janus colloids,[31–41] in which half of the molecular surface is attractive and the other half is repulsive. The molecular geometry and interactions involved in the HS–SW model allow only for a limited number of bonds to be developed. Such a "limited-valence" class of models has received significant attention in the last few years; in particular it has been demonstrated that, upon decreasing the valence below six, the liquid–vapor unstable region progressively shrinks to lower densities, thereby creating an intermediate region where a stable network may be formed,[42,43] giving rise to equilibrium gels.[44] In order to further elucidate the differences in the phase behavior between the SW–SW and HS–SW models, we also study a series of intermediate models, obtained by progressively reducing to zero one of the square-well interactions of the original SW–SW model. For the sake of completeness, and for comparison with previous models, we also shortly revisit the structural properties of the tangent hard spheres model (HS–HS model), previously investigated by some of us and other authors (see ref. 45–48 and references therein).

Integral equations theories of the liquid state[49] play a significant role in the study of simple and complex fluids, being relatively simple to implement and generally able to provide a good description of fluid-phase equilibria.[50] In our study we adopt the Reference Interaction Site Model (RISM) theory of molecular fluids, developed by Chandler and Andersen[51] as a generalization of the Ornstein–Zernike theory of simple fluids.[49] In the original formulation, molecules were viewed as composed by a suitable superposition of several hard spheres, rigidly bonded together so as to reproduce a given molecular geometry.[52] Later on, the theory has been extended to deal with a more realistic representation of complex liquids, including associating fluids such as water,[53,54] or methanol.[55–57] Recently, we have developed a thermodynamically self-consistent RISM approach, able to positively predict the structural properties of homonuclear hard dumbbells.[45,46] RISM has been widely used in the study of colloidal models as, for instance, to characterize the thermodynamic and structural properties of discotic lamellar colloids,[58,59] the self-assembly in diblock copolymers (modeled as "ultrasoft" colloids),[60] the interaction between colloidal particles and macromolecules,[61] the crystallization and solvation properties of nanoparticles in aqueous solutions,[62] the liquid structure of tetrahedral colloidal particles[63] and the self-assembly properties of Janus rods.[64]

In this work, we have systematically assessed our theoretical predictions for the structural properties of various models against standard Monte Carlo simulations. RISM results concerning the fluid phase equilibria have been compared with Successive Umbrella Sampling (SUS[65]) simulations, coupled with histogram reweighting techniques.[66]

The paper is organized as follows: in the next section we give details of the model, the RISM theory and the plan of simulations. Results are presented and discussed in the third section. Conclusions follow in the last section.

Model, theory and simulation

A schematic representation of all models studied in this work is shown in Fig. 1; the SW–SW dumbbell is constituted by two tangent hard spheres of diameter σ, interacting with the sites of another dumbbell *via* identical square-well attractions, *i.e.*

$$V_{11}(r) = V_{12}(r) = V_{22}(r) \equiv V_{SW}(r) \quad (1)$$

where 1 and 2 label the two interaction sites and

$$V_{SW}(r) = \begin{cases} \infty & \text{if } 0 < r < \sigma \\ -\varepsilon & \text{if } \sigma \le r < \sigma + \lambda\sigma \\ 0 & \text{otherwise.} \end{cases} \quad (2)$$

Besides the hard-core diameter σ, the potential in eqn (2) is characterized by the range λ and the depth ε of the square-well interaction. The parameters σ and ε provide, respectively, the unit of length and energy, in terms of which we define the reduced temperature $T^* = k_B T/\varepsilon$ (with k_B as the Boltzmann constant), pressure, $P^* = P\sigma^3/\varepsilon$ and density, $\rho^* = \rho\sigma^3$. The packing fraction is defined as $\phi = \rho\nu$ where ν is the molecular volume, *i.e.* $\phi = (\pi/3)\rho\sigma^3$. In all calculations we have fixed $\lambda = 0.1$.

In the HS–SW model, the square-well attraction on site 1 is switched off, so that the mutual interactions among sites on different molecules now read:

$$V_{11}(r) = V_{12}(r) \equiv V_{HS}(r);\ V_{22}(r) \equiv V_{SW}(r) \quad (3)$$

where $V_{HS}(r)$ is the hard-sphere potential of diameter σ.

As for the intermediate models connecting the SW–SW and HS–SW ones, they have been obtained by progressively reducing the square-well depth of site 1, from $\varepsilon = 1$, corresponding to the SW–SW model, to $\varepsilon = 0$, corresponding to the HS–SW model.

Finally we have studied a pure HS–HS model (tangent homonuclear hard dumbbell) as a necessary benchmark to test the quality of our theoretical approach, as well as a starting point to characterize the properties depending mainly on packing effects; for the HS–HS interaction:

$$V_{11}(r) = V_{12}(r) = V_{22}(r) \equiv V_{HS}(r). \quad (4)$$

As far as the RISM theoretical framework is concerned, the pair structure of a fluid composed by identical molecules, each formed by n interaction sites is characterized by a set of

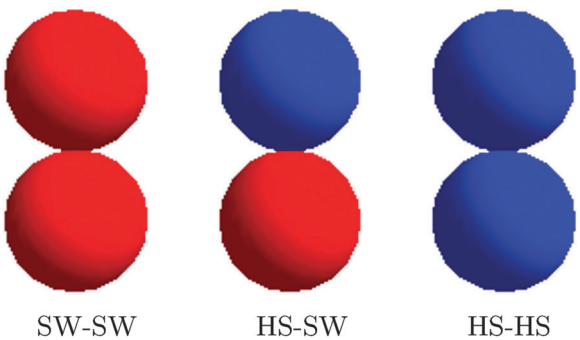

Fig. 1 Sketch of molecular models studied in this work. Blue and red spheres indicate HS and SW sites, respectively.

$n(n+1)/2$ site–site intermolecular pair correlation functions $h_{ij}(r) = g_{ij}(r) - 1$, where $g_{ij}(r)$ are the site–site radial distribution functions. The $h_{ij}(r)$ are related to a set of intermolecular direct correlation functions $c_{ij}(r)$ by a matrix equation that in k-space reads:

$$\mathbf{H}(k) = \mathbf{W}(k)\mathbf{C}(k)\mathbf{W}(k) + \rho\mathbf{W}(k)\mathbf{C}(k)\mathbf{H}(k). \quad (5)$$

For the two-site models investigated in this work ($i, j = 1,2$) and therefore in eqn (5) $\mathbf{H} \equiv [h_{ij}(k)]$, $\mathbf{C} \equiv [c_{ij}(k)]$, and $\mathbf{W} \equiv [w_{ij}(k)]$ are 2×2 symmetric matrices; the elements $w_{ij}(k)$ are the Fourier transforms of the intramolecular correlation functions, written explicitly as:

$$w_{ij}(k) = \frac{\sin[kL_{ij}]}{kL_{ij}}, \quad (6)$$

where in our case the bond length L_{ij} is given either by $L_{ij} = \sigma$, if $i \neq j$, or by $L_{ij} = 0$, otherwise. We have complemented the RISM equation by the HNC closure[49] for the direct correlation functions $c_{ij}(r)$:

$$c_{ij}(r) = \exp[-\beta V_{ij}(r) + \gamma_{ij}(r)] - \gamma_{ij}(r) - 1 \quad (7)$$

where $\beta = 1/T^*$, $V_{ij}(r)$ are the site–site potentials of eqn (1)–(4) and $\gamma_{ij}(r) = h_{ij}(r) - c_{ij}(r)$. We have implemented the numerical solution of the RISM/HNC scheme by means of a standard iterative Picard algorithm, on a mesh of 8192 points with a spacing $\Delta r = 0.005\sigma$.

As for the determination of fluid phase equilibria in the RISM framework, we have calculated the excess free-energy *via* thermodynamic integrations along constant-density paths according to:[49]

$$\frac{\beta A^{ex}(\beta)}{N} = \frac{\beta A^{ex}(\beta = 0)}{N} + \int_0^\beta \frac{U(\beta')}{N} d\beta', \quad (8)$$

where N is the number of molecules and the internal energy of the system is given by:

$$\frac{U}{N} = 2\pi\rho \sum_{i,j=1}^{2} \int_0^\infty V_{ij}(r) g_{ij}(r) r^2 dr. \quad (9)$$

In eqn (8) A^{ex} ($\beta = 0$) corresponds to the excess free energy of the HS–HS model, for which we have used the analytic expression fitting the Monte Carlo data derived by Tildesley and Streett.[47] Once the free energy is known, the pressure can be deduced by derivation according to:

$$\frac{\beta P}{\rho} = \rho \left.\frac{\partial(\beta A/N)}{\partial\rho}\right|_T. \quad (10)$$

In order to apply eqn (10), we have first performed a polynomial best-fit of the free energy as a function of the density for each temperature; then, we have calculated the derivative of such analytical functions to get the pressure and in turn the chemical potential, according to the standard thermodynamic relation:

$$\beta\mu = \frac{\beta A}{N} + \frac{\beta P}{\rho}. \quad (11)$$

Finally, the requirement of equal P and μ at fixed T in both phases determines the coexisting densities at a given temperature.

Actually, the RISM/HNC formulation provides another straightforward, closed expression for the free energy, requiring no thermodynamic integration, as detailed in ref. 67 and 68. However, a preliminary application of such a closed formula for the SW–SW and HS–SW models (not reported in the paper) has shown that the free energy estimates thereby obtained are less accurate in comparison with those calculated according to the more cumbersome scheme of eqn (8)–(11). The fact that various routes from structure to thermodynamics yield different predictions is not surprising, given the thermodynamic inconsistency of most integral equation theories, including the RISM/HNC scheme. In this context, it is generally recognized that the energy route provides the most accurate predictions (see ref. 50 and references therein). Then, the integration/derivation calculations involved in eqn (8) and (10) can be accurately carried out by analyzing the temperature range over sufficiently narrow steps.

As far as simulations are concerned, we have calculated structural and thermodynamic properties of our models by means of standard Monte Carlo (MC) simulations at constant volume and temperature (NVT ensemble), on a system constituted by $N = 2048$ particles enclosed in a cubic box with standard periodic boundary conditions. As for the coexistence curves, they have been evaluated *via* successive umbrella sampling (SUS) simulations[65] in the grand canonical (μVT) ensemble. According to this method, the range $[0,N_{max}]$ of particles is divided into many small windows of size ΔN. For each window i in the interval $N \in [N_i, N_i + \Delta N]$, a grand-canonical MC simulation is carried out, avoiding the insertion or deletion of particles outside the range of the window.[69] This allows the calculation of the histogram H_i monitoring how often a state with N particles is visited in the window i. The full probability density is then calculated as the following product:

$$\frac{P(N)}{P(0)} = \frac{H_0(1)}{H_0(0)} \cdot \frac{H_0(2)}{H_0(1)} \cdots \frac{H_0(\Delta N)}{H_0(\Delta N - 1)} \cdots \frac{H_i(N)}{H_i(N-1)} \quad (12)$$

The advantage of using such a method lies both in the possibility to sample all microstates without any biasing function and in the relative simplicity to parallelize the run, with a speed gain scaling linearly with the number of processors. Once $P(N)$ is obtained, at fixed temperature and chemical potential, histogram reweighting techniques[66] can be applied to eventually obtain the coexistence points. This is done by reweighting the densities histogram until the regions below the two peaks (in the low- and high-density phases) attain the same area.

Results and discussion

Structure factors

We first recall that, as shown in our previous papers,[45,46] the RISM approach provides generally good results for the HS–HS fluid. Here we show in Fig. 2 a comparison between RISM and MC site–site structure factors $S_{ij}(k)$ for two different densities, $\rho^* = 0.2$ and $\rho^* = 0.4$ (corresponding to the packing fractions $\phi \simeq 21\%$ and $\phi \simeq 42\%$, respectively). The agreement is good for both densities, with RISM able to predict the structuring of the $S_{ij}(k)$ as the density increases. The main peak at $k\sigma \approx 6.5$, clearly visible at $\rho^* = 0.4$ suggests a geometrical arrangement in

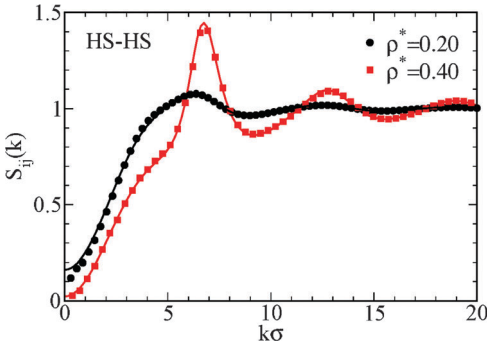

Fig. 2 MC (symbols) and RISM (lines) site–site structure factors $S_{ij}(k)$ for the HS–HS fluid at two different densities. Note that $S_{11}(k) = S_{12}(k) = S_{22}(k)$ due to the symmetry of the model.

which two dumbbells are closely packed, with each sphere of a dumbbell linked in a close configuration with the spheres of another dumbbell. This geometry is compatible with the relatively high value of the packing fraction and constantly emerges in the site–site correlations of all models. On the other hand, since the structuring of $S_{ij}(k)$ is exclusively driven by packing effects, the related features tend to vanish when the density decreases: at $\rho^* = 0.2$ only a small shoulder in $S_{ij}(k)$ is visible, reminiscent of the well defined peak observed at $\rho^* = 0.4$.

A different behavior is expected for the SW–SW fluid; in particular, due to the isotropy of both molecular geometry and interaction potential, we expect a standard gas–liquid phase separation to take place below a certain critical temperature. Indeed, as visible from Fig. 3a, at high temperature ($T^* = 0.70$), the behavior of $S_{ij}(k)$ closely resembles the HS–HS situation, especially at high density. Then, as the temperature is lowered, the $k \to 0$ limit of $S_{ij}(k)$ remarkably increases at $\rho^* = 0.2$ (see Fig. 3b), signaling a possible approach to a gas–liquid phase separation, as we shall further comment below. Such a feature disappears at high density, because packing effects tend to suppress density fluctuations on a large-distance scale. Also for the SW–SW model, RISM predictions faithfully reproduce MC results by proving to be able, in particular, to follow the observed increase of $S_{ij}(k \to 0)$.

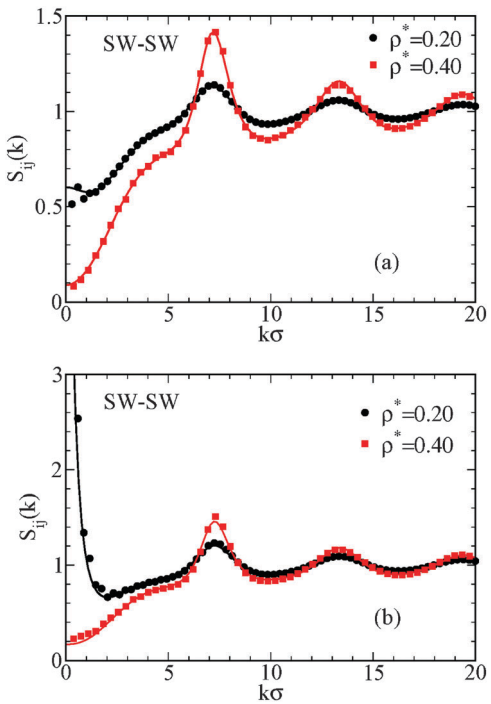

Fig. 3 MC (symbols) and RISM (lines) $S_{ij}(k)$ for the SW–SW fluid at $T^* = 0.70$ (a) and $T^* = 0.55$ (b) at two different densities. Note that $S_{11}(k) = S_{12}(k) = S_{22}(k)$ due to the symmetry of the model.

A third physical scenario is observed for the HS–SW fluid. Site–site structure factors at different temperatures ($T^* = 0.55$ and 0.30) and densities ($\rho^* = 0.2$ and 0.4) are reported in Fig. 4 where, due to the different interaction sites, three curves are explicitly displayed. The presence of only one attractive interaction (positioned on site 2 of the dumbbell) has a deep influence on the structure of the fluid: in all panels of Fig. 4 we observe the presence and progressive enhancement of a low-k peak in $S_{22}(k)$, at $k\sigma \sim 2$ – besides the main correlation peak at $k\sigma \sim 6.5$ – and the simultaneous absence of any diverging trend in the $k \to 0$ limit of all $S_{ij}(k)$. This evidence is compatible with a physical picture in which dumbbells tend to self-aggregate, forming clusters out of the homogeneous fluid as the temperature decreases. Indeed it has been shown that the development of a low-k peak is correlated to the formation of aggregates both in experiments, as for instance in colloid–polymer mixtures and globular protein solutions (see *e.g.* ref. 70 and 71), as well as in theoretical and numerical investigations of model fluid with microscopic competing interactions (see *e.g.* ref. 72 and 73 and references). Recently, such a feature in the structure factor has been more generally related to the presence of some kind of "intermediate-range order" in the fluid.[74,75] In our case, the presence of stable clusters clearly emerges also by visual inspection of the equilibrated MC configurations (see next Fig. 12). Also in this case, RISM positively predicts all structural features, and in particular the progressive enhancement of the low-k peak: only at low temperature and density (see Fig. 4c), RISM yields a less structured $S_{22}(k)$ in comparison with the MC datum. This can be explained by the difficulty the RISM faces to reproduce the structure of a fluid that turns progressively non-homogeneous, as signaled for instance by the pronounced height of the low-k peak visible in Fig. 4c.

An interesting feature emerging from Fig. 4 – and particularly well documented in panel (d) – is the development of a pronounced negative minimum in $S_{12}(k)$ as the temperature decreases and the density increases, accompanied by the progressive alignment between such a minimum and the corresponding peaks of $S_{11}(k)$ and $S_{22}(k)$. Such a behavior amounts to a substantially equal pace in the ordering of the HS and SW sites of the dumbbells. A similar alignment in the structure factors is known to take place in two-component ionic fluids where an alternate order of oppositely charged particles emerges, so as to cope with charge neutrality constraints (see ref. 76 for a detailed illustration). In the present case, the alignment may be attributed to the combined effect of energy minimization, achieved *via* the clustering of SW sites, with the ensuing drag imposed on the rigidly linked HS site.

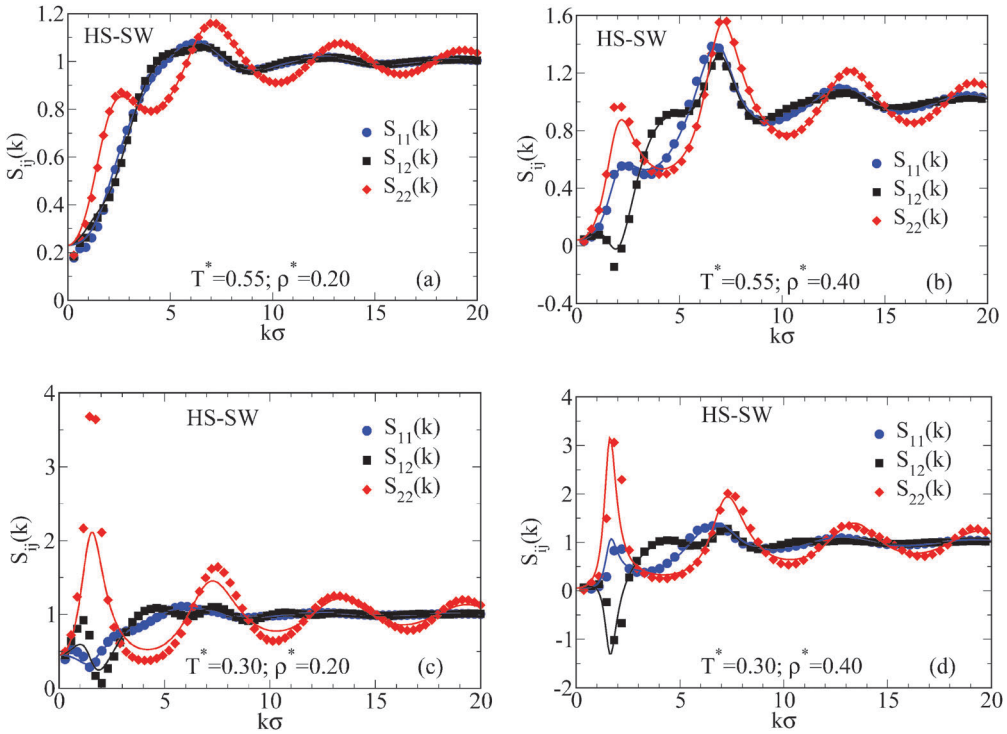

Fig. 4 MC (symbols) and RISM (lines) $S_{ij}(k)$ for the HS–SW fluid at different temperatures and densities (see legends). Subscripts 1 and 2 refer to the HS and SW site, respectively.

We complete our structural investigation of the HS–SW fluid with Fig. 5, where we show the behavior of the molecular centre–centre structure factor, $S_{cc}(k)$, at fixed density, $\rho^* = 0.2$, and various temperatures. In the figure, the development of the low-k peak is visible even in the $S_{cc}(k)$, though this feature is smoother than that observed in the corresponding $S_{22}(k)$. We report only MC results, since centre–centre correlations can be included in the RISM formalism for the two-site model at the cost of introducing a "ghost site" (*i.e.* bearing no interactions) to represent the centre of the molecule; we have avoided such a procedure since previous studies[77] have shown that the presence of ghost sites spuriously influences the behavior of correlations involving the remaining "real" sites.

Free energy and phase equilibria

According to the procedure described in the previous section – see eqn (8) and (9) – the starting point for the determination of fluid phase equilibria in the RISM formalism is the calculation of the internal energy along several isotherms. Three examples of such calculations for the SW–SW model at high, intermediate and low temperatures are reported in Fig. 6: we see that theoretical predictions are in close agreement with simulation data at $T^* = 0.70$ and $T^* = 0.60$, whereas small discrepancies appear at low temperature, *i.e.* at $T^* = 0.55$.

In Fig. 7 we report RISM predictions for the free energy and pressure, calculated according to eqn (8)–(10), as functions of the density along several isotherms. The monotonic increase of the free energy at high temperatures is progressively smoothed

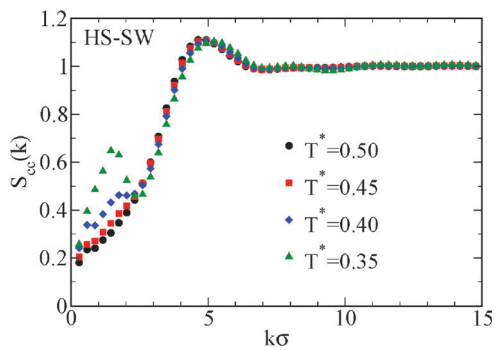

Fig. 5 MC centre–centre structure factors for the HS–SW fluid at fixed $\rho^* = 0.2$ and different temperatures.

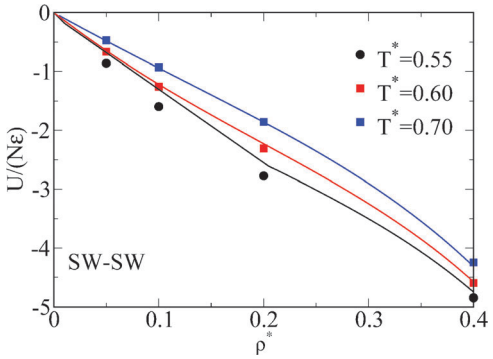

Fig. 6 MC (symbols) and RISM (lines) internal energy per particle for the SW–SW fluid at high, intermediate and low temperatures.

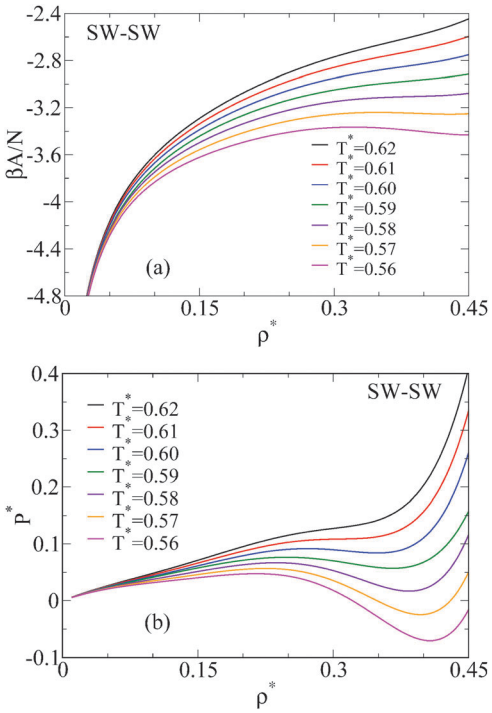

Fig. 7 RISM free energy (a) and pressure (b) for the SW–SW fluid as functions of the density along several isotherms.

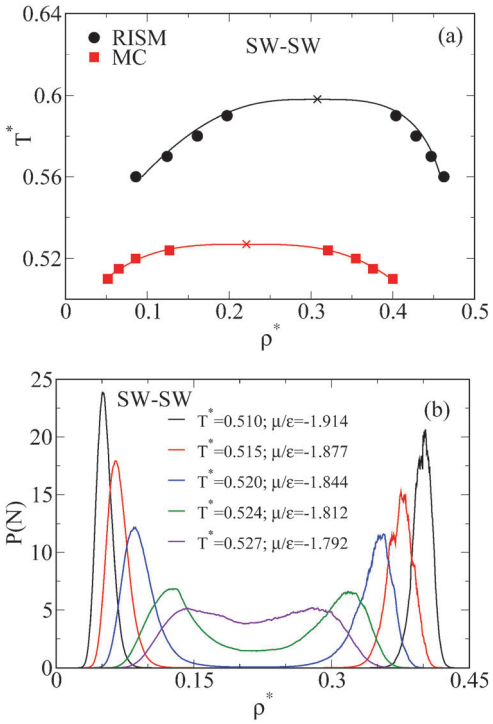

Fig. 8 Panel a: RISM (circles) and MC (squares) gas–liquid coexistence points for the SW–SW fuid; full lines are best-fits calculated according to the scaling law for the densities and the law of rectilinear diameters; the critical points obtained by such best-fits are indicated by crosses. Panel b: histograms of the probability $P(N)$ to find the system with N particles in the simulation box for various temperatures and chemical potentials, as obtained by SUS grand-canonical simulations. The box length is 13.57σ.

by the appearance of a flat portion at $T^* = 0.57$, heralding a bend towards lower values at $T^* = 0.56$. The pressure exhibits a van der Waals loop at $T^* = 0.60$ that becomes progressively more pronounced upon lowering the temperature. This evidence provides a clear indication of the value of the critical temperature.

RISM predictions for the gas–liquid coexistence points of the SW–SW model are reported in Fig. 8a, along with corresponding MC data. As for the latter, MC distributions of densities in the μVT ensemble are plotted in Fig. 8b, where we show that, starting from an almost homogeneous distribution at $T^* = 0.527$, two well defined peaks develop upon cooling the system, corresponding to the densities of the gas and liquid phases. As visible from Fig. 8a, the RISM turns out to overestimate the gas–liquid coexistence curve, in agreement with a previous study on the same model with $\lambda = 0.5$,[18] where the RISM was coupled with a Mean Spherical Approximation closure. We have calculated the RISM and MC critical temperature and density from corresponding coexistence points, through the scaling law for the densities and the law of rectilinear diameters with an effective critical exponent $\beta = 0.32$.[78] Results of such best-fit procedures, also reported in Fig. 8a, are: $T_{crit}^* = 0.598$ and $\rho_{crit}^* = 0.307$ for RISM, and $T_{crit}^* = 0.527$ and $\rho_{crit}^* = 0.221$ for MC. Notwithstanding the relative discrepancies, both RISM theory and MC simulations provide a picture of the SW–SW model as a standard isotropic fluid, thus confirming the indications coming from the structural analysis about the existence of a gas–liquid phase separation.

As far as the HS–SW model is concerned, RISM and MC results for the internal energy are reported in Fig. 9. As in the previous case, a good agreement between theory and simulations is found at relatively high ($T^* = 0.55$) and intermediate ($T^* = 0.40$) temperatures whereas RISM underestimates (the absolute value of) the internal energy at low temperature, $T^* = 0.30$. This evidence may be a consequence of what is observed for $S_{22}(k)$ in Fig. 4c: the underestimation of the low-k peak of such a site–site structure factor, highlighted at $\rho^* = 0.2$, implies a similar behavior of the relative site–site radial distribution function intervening in the expression for the internal energy in eqn (9).

RISM free energies and pressures for the HS–SW fluid are reported in Fig. 10, as functions of the density along several isotherms. All free energy curves exhibit a monotonic trend to

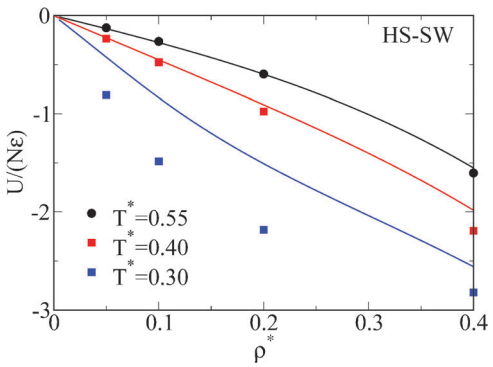

Fig. 9 MC (symbols) and RISM (lines) internal energy per particle for the HS–SW fluid at high, intermediate and low temperatures.

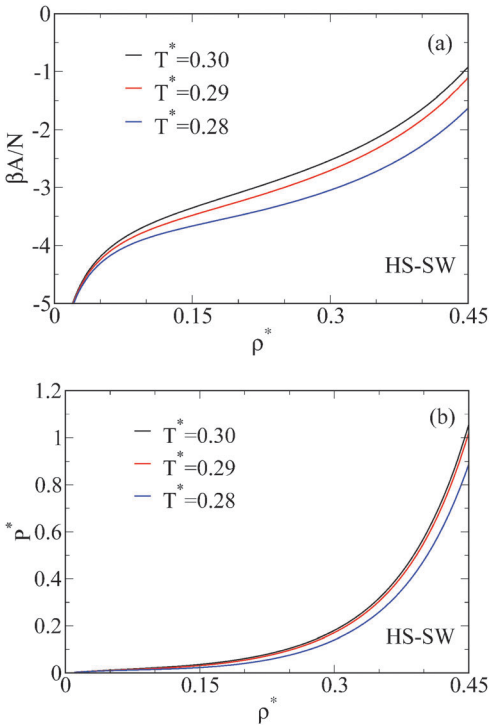

Fig. 10 RISM free energy (a) and pressure (b) for the HS–SW fluid as functions of the density along several isotherms.

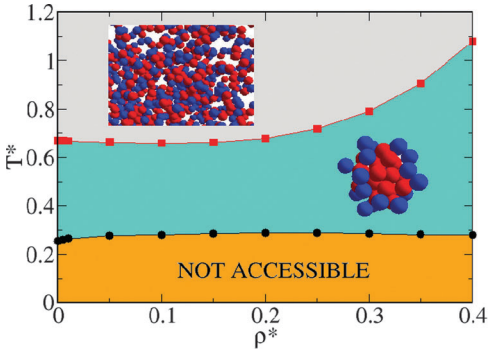

Fig. 11 RISM predictions for the phase behavior of the HS–SW fluid (symbols). The grey area is separated from the cyan zone by a border line identified by the appearance of the low-k peak in the $S_{22}(k)$. Snapshots taken from MC simulations schematically illustrate the different arrangements of the fluid across the border line with red and blue spheres indicating SW and HS sites, respectively. The underlying orange area is out of operational conditions for RISM calculations.

increase, with no appreciable concavity changes all over the investigated temperature range. As a consequence, pressure does not exhibit any van der Waals loop, suggesting a supercritical behavior of the HS–SW model down to $T^* = 0.28$; the convergence of the RISM numerical algorithm eventually fails immediately below this temperature. Such a RISM picture is coherent with the MC observation: down to $T^* = 0.20$, *i.e.* the lowest temperature for which we have been able to equilibrate the fluid, SUS does not show any double-peak behavior in the probability density $P(N)$, ruling out the existence of a gas–liquid phase separation for $T^* > 0.20$. Below such a temperature MC results are not available, due to the exceedingly long computational time required to equilibrate the system.

Collecting structural and thermodynamic observations, the phase behavior of the HS–SW model is summarized in Fig. 11, where the RISM predictions for the first appearance of the low-k peak in $S_{22}(k)$ are also reported. As visible, such predicted values form a border line separating a region in the $T^* - \rho^*$ diagram where a pure homogeneous fluid exists, at high temperatures, from another region, at lower temperatures, where a locally non-homogeneous cluster fluid exists. We have determined such a border line within the RISM approach, since the theoretical scheme yields, as discussed in Fig. 4, accurate structural predictions in this temperature regime; moreover, RISM allows – in comparison with MC calculations – for a finer spanning of different thermodynamic conditions and for a more accurate observation of the early development of the low-k peak. We note that the temperature for the first appearance of the low-k peak in $S_{22}(k)$ hardly changes at low and intermediate densities, keeping an almost constant value ~ 0.7. Conversely, when $\rho^* > 0.2$ the low-k peak develops at progressively higher temperatures, signaling that the density increase promotes the formation of self-assembled structures in the system. For completeness, we also report in Fig. 11 the low-temperature regime out of operational conditions for RISM calculations.

Snapshots of typical configurations taken from MC simulations at high and low temperatures and densities are shown in the four panels of Fig. 12; the different $T^* - \rho^*$ values are chosen so as to be close to the upper (panels a and b) and lower (panels c and d) limits of the cyan region depicted in Fig. 11. At $T^* = 0.55$ clusters are not developed enough to be seen by a straightforward visual inspection, both at low ($\rho^* = 0.05$, panel a) and high ($\rho^* = 0.4$, panel b) densities. A different scenario emerges at $T^* = 0.25$: at low density ($\rho^* = 0.05$, panel c), isolated clusters of almost spherical shape, constituted by a variable number of dumbbells, are clearly visible, confirming the indications given by the static structure factors. A different geometrical arrangement is instead observed at high density, ($\rho^* = 0.4$, panel d), with dumbbells forming macro-domains almost spanning the simulation box.

To summarize, convergent thermodynamic and structural evidence, coming from theory and simulations, possibly suggests that in the HS–SW fluid the self-assembly process inhibits the gas–liquid phase separation, or at least shrinks such a phase separation into a region of the phase diagram narrow enough to be inaccessible both to RISM and MC. To further elucidate this point, we have studied the phase behavior of several intermediate models between the SW–SW and the HS–SW ones. Specifically, we have calculated the critical points of SW–SW models in which the square-well depth of site 1, ε_1, is progressively turned from one to zero. In this way, the case $\varepsilon_1 = 1$ corresponds to the original SW–SW model whereas, at the opposite limit, $\varepsilon_1 = 0$, we recover the HS–SW model. In Fig. 13 we show the RISM and MC critical temperatures as functions of ε_1: remarkably, the two sets of data lie on almost parallel straight lines, with a constant discrepancy of ~ 0.06 in the predicted values of T_{crit}^*. Numerical values of MC and RISM critical parameters are reported in Table 1, along with the relative error bars. By comparing the

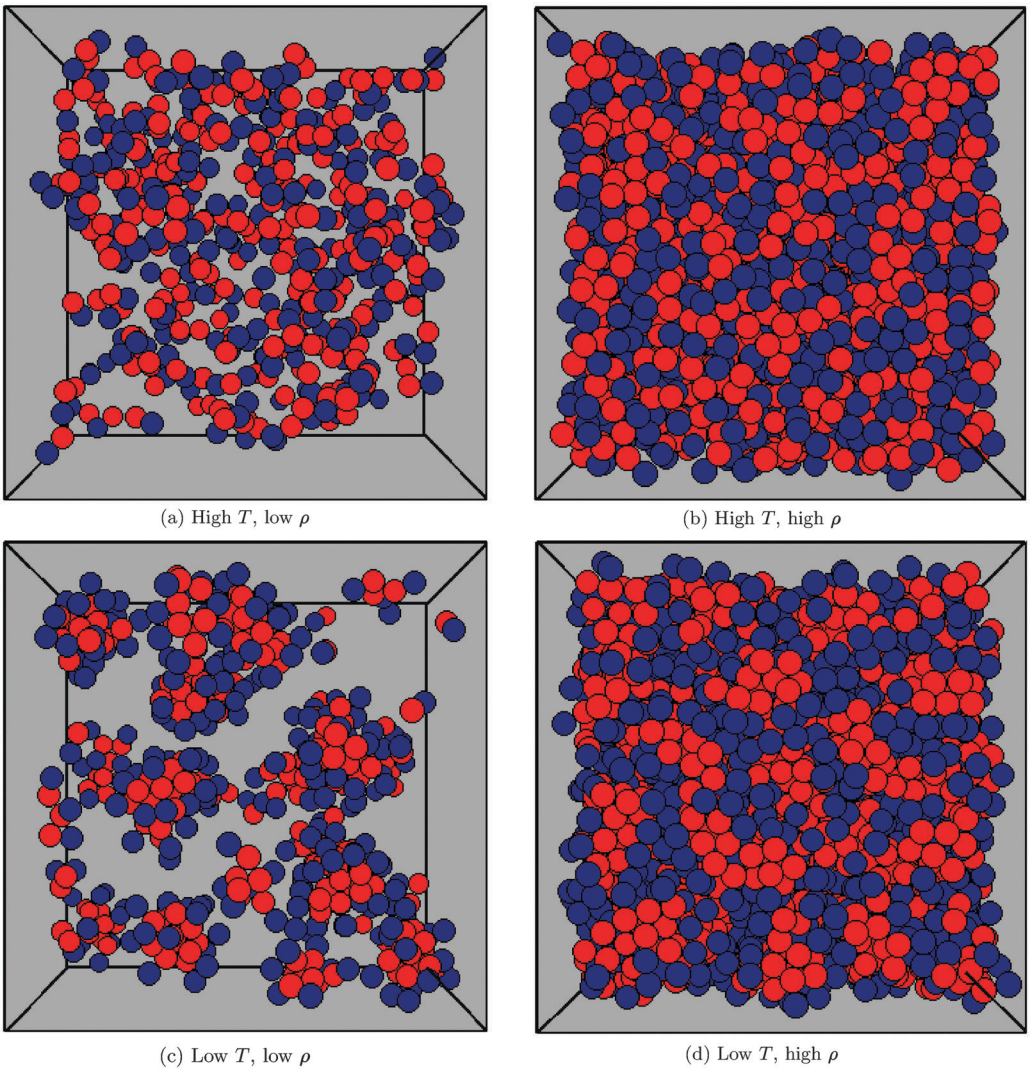

Fig. 12 Snapshots of typical configurations of the HS–SW fluid: T^* = 0.55, ρ^* = 0.05 (a): T^* = 0.55, ρ^* = 0.4 (b); T^* = 0.25, ρ^* = 0.05 (c): T^* = 0.25, ρ^* = 0.4 (d). Blue and red spheres indicate HS and SW sites, respectively.

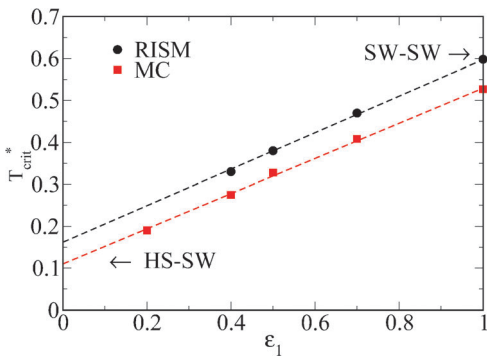

Fig. 13 RISM (circles) and MC (squares) critical temperatures of intermediate SW–SW models with variable ε_1. Lines are linear fits of calculated points.

Table 1 Critical parameters for the SW–SW models with variable ε_1. RISM and MC error bars correspond to the uncertainties by which we have appreciated the development, respectively, of a van der Waals loop in the pressure (see Fig. 7b) and a double peak in the $P(N)$ (see Fig. 8b)

ε_1	T^*	ρ^*	μ/ε
MC			
1.0	0.527 ± 0.001	0.22 ± 0.01	−1.813
0.7	0.408 ± 0.002	0.21 ± 0.01	−1.453
0.5	0.328 ± 0.003	0.19 ± 0.02	−1.377
0.4	0.275 ± 0.005	0.23 ± 0.01	−1.729
0.2	0.190 ± 0.010	0.22 ± 0.02	−2.055
RISM			
1.0	0.60 ± 0.01	0.31 ± 0.05	−1.476
0.7	0.47 ± 0.01	0.30 ± 0.05	−1.128
0.5	0.38 ± 0.01	0.29 ± 0.05	−1.063
0.4	0.33 ± 0.01	0.30 ± 0.05	−1.127

trends of T_{crit}^* and ρ_{crit}^*, both RISM and MC document that T_{crit}^* decreases upon lowering ε_1, whereas ρ_{crit}^* keeps generally constant almost independently of the specific value of ε_1. Extrapolating to ε_1 = 0, we obtain for the putative critical temperature of the HS–SW model $T_{crit}^* \sim 0.16$ and ~ 0.10 from

RISM and MC, respectively. Such values are out of the operational range of both integral equations and simulation techniques adopted here. Interestingly enough, RISM predictions for $S_{22}(k)$ (not reported here) show that at fixed density the diverging trend in the $k \to 0$ limit appears at lower temperatures upon decreasing ε_1. At the same time, the low-k peak manifests itself only as a small shoulder at high ε_1 and becomes progressively more sharpened as ε_1 decreases. Remarkably, this evidence – along with the critical temperature data – provides us with the picture of a dumbbell model fluid continuously changing its phase behavior by simply tuning the strength of attraction on one of the two interaction sites.

Conclusions

We have investigated by the RISM/HNC integral equation theory and MC simulations the structural and thermodynamic properties of different colloidal dumbbells. Specifically, we have studied a model composed by two identical tangent hard spheres surrounded by two identical short-range square-well interactions (SW–SW model), and a second model in which only one square-well interaction is present (HS–SW model). We have also characterized the phase behavior of a series of intermediate models, by progressively reducing the square-well depth on one of the two sites of the SW–SW model, and, for completeness, the structural properties of the tangent homonuclear hard dumbbell fluid.

We have analyzed the phase behavior and gas–liquid equilibria by employing the energy route from structure to thermodynamics in the RISM framework, since the more straightforward HNC closed formulæ turn to be less reliable in our case. As for the simulation approach, we have carried out successive umbrella sampling calculations to obtain the pressure and chemical potential. RISM and MC agree in documenting two completely different physical scenarios for the SW–SW and HS–SW models. As for the former, we have found a standard gas–liquid coexistence curve, with the RISM theory slightly overestimating the critical temperature and density in comparison with simulation data. MC structure factors are well reproduced by RISM, suggesting that the isothermal compressibility is generally well predicted. As for the HS–SW model, the appearance and growth of a low-k peak in the static structure factor signal the development of a locally non-homogeneous cluster fluid. At low temperatures the formation of such aggregates plausibly inhibits the gas–liquid phase separation and gives rise to a fluid constituted by well defined, essentially non-interacting clusters. RISM and MC calculations concerning the intermediate models between SW–SW and HS–SW show a linear decrease of the critical temperature as a function of the square-well depth. A straightforward extrapolation of such data predicts that, should a critical temperature exist for the HS–SW model, it would be low enough to fall out of RISM and MC operational ranges.

The models investigated in this work exhibit a rich phase behavior, including the presence of phase separation and self-assembly processes. Such models are characterized by a relatively simple design; moreover we have documented how reliable predictions concerning their structural and thermodynamic properties can be obtained within the RISM theoretical framework. Such desirable and advantageous properties set the SW–SW, HS–SW and intermediate models as ideal candidates to elucidate the effects of tunable attractive interactions on the cluster formation and self-assembly of colloidal dumbbells. Further investigations of colloidal dumbbells, including different square-well widths and hard-sphere sizes, are currently in progress and will constitute the subject of forthcoming works.

Acknowledgements

We gratefully acknowledge support from ERC-226207-PATCHY-COLLOIDS and the PRIN-MIUR 2010–2011 project, within which this work has been carried out. We also thank Patrick O'Toole and Toby Hudson for useful discussions and on-going collaboration.

References

1 S. Sacanna and D. J. Pine, *Curr. Opin. Colloid Interface Sci.*, 2011, **16**, 96.
2 A. P. R. Eberle, R. Castañeda-Priego, J. M. Kim and N. J. Wagner, *Langmuir*, 2012, **28**, 1866.
3 Q. Meng, Y. Kou, X. Ma, Y. Liang, L. Guo, C. Ni and K. Liu, *Langmuir*, 2012, **28**, 5017.
4 T. H. Zhang, J. Klok, R. H. Tromp, J. Groenewold and W. K. Kegel, *Soft Matter*, 2012, **8**, 667.
5 Q. Chen, J. Yan, J. Zhang, S. C. Bae and S. Granick, *Langmuir*, 2012, **28**, 1355.
6 J. Yan, M. Bloom, S. C. Bae, E. Luijten and S. Granick, *Nature*, 2012, **491**, 578.
7 A. Yethiraj and A. van Blaaderen, *Nature*, 2003, **421**, 513.
8 J.-W. Kim, R. J. Larsen and D. A. Weitz, *J. Am. Chem. Soc.*, 2006, **128**, 14374.
9 E. Lee, Y.-H. Jeong, J.-K. Kim and M. Lee, *Macromolecules*, 2007, **40**, 8355.
10 I. D. Hosein and C. M. Liddell, *Langmuir*, 2007, **23**, 10479.
11 D. Zerrouki, J. Baudry, D. Pine, P. Chaikin and J. Bibette, *Nature*, 2008, **455**, 381.
12 D. Nagao, C. M. van Kats, K. Hayasaka, M. Sugimoto, M. Konno, A. Imhof and A. van Blaaderen, *Langmuir*, 2010, **26**, 5208.
13 S. Chakrabortty, J. A. Yang, Y. M. Tan, N. Mishra and Y. Chan, *Angew. Chem.*, 2010, **49**, 2888.
14 J. D. Forster, J. G. Park, M. Mittal, H. Noh, C. F. Schreck, C. S. O'Hern, H. Cao, E. M. Furst and E. R. Dufresne, *ACS Nano*, 2011, **5**, 6695.
15 D. Nagao, M. Sugimoto, A. Okada, H. Ishii, M. Konno, A. Imhof and A. van Blaaderen, *Langmuir*, 2012, **28**, 6546.
16 K. Yoon, D. Lee, J. W. Kim, J. Kim and D. A. Weitz, *Chem. Commun.*, 2012, **48**, 9056.
17 K. Yoon, PhD thesis, Harvard University, 2012, http://nrs.harvard.edu/urn-3:HUL.InstRepos:9767979.
18 A. Yethiraj and C. K. Hall, *Mol. Phys.*, 1991, **72**, 619.
19 M. P. Taylor, J. Luettmer-Strathmann and J. E. G. Lipson, *J. Chem. Phys.*, 2001, **114**, 5654.

20 N. Wu and Y. C. Chiew, *J. Chem. Phys.*, 2001, **115**, 6641.
21 S. H. Chong, A. J. Moreno, F. Sciortino and W. Kob, *Phys. Rev. Lett.*, 2005, **94**, 215701.
22 A. J. Moreno, S. H. Chong, W. Kob and F. Sciortino, *J. Chem. Phys.*, 2005, **123**, 204505.
23 M. Marechal and M. Dijkstra, *Phys. Rev. E*, 2008, **77**, 061405.
24 M. A. Miller, R. Blaak, C. N. Lumb and J. P. Hansen, *J. Chem. Phys.*, 2009, **130**, 114507.
25 G. A. Chapela and J. Alejandre, *J. Chem. Phys.*, 2010, **132**, 104704.
26 R. Ni and M. Dijkstra, *J. Chem. Phys.*, 2011, **134**, 034501.
27 M. Marechal, H. H. Goetzke, A. Härtel and H. Löwen, *J. Chem. Phys.*, 2011, **135**, 234510.
28 P. Ilg and E. D. Gado, *Soft Matter*, 2011, **7**, 163.
29 G. A. Chapela, F. de Rio and J. Alejandre, *J. Chem. Phys.*, 2011, **134**, 224105.
30 C. Y. Zhang, X. L. Jian and W. M. Ding, *EPL*, 2012, **100**, 38004.
31 A. M. Jackson, J. W. Myerson and F. Stellacci, *Nat. Mater.*, 2004, **3**, 330.
32 K.-H. Roh, D. C. Martin and J. Lahann, *Nat. Mater.*, 2005, **4**, 759.
33 B. Wang, B. Li, B. Zhao and C. Y. Li, *J. Am. Chem. Soc.*, 2008, **130**, 11594.
34 L. Hong, A. Cacciuto, E. Luijten and S. Granick, *Langmuir*, 2008, **24**, 621.
35 A. Walther and H. Müller, *Soft Matter*, 2008, **4**, 663.
36 C.-H. Chen, R. K. Shah, A. R. Abate and D. A. Weitz, *Langmuir*, 2009, **25**, 4320.
37 F. Sciortino, A. Giacometti and G. Pastore, *Phys. Rev. Lett.*, 2009, **103**, 237801.
38 B. S. Jiang, Q. Chen, M. Tripathy, E. Luijten, K. Schweizer and S. Granick, *Adv. Mater.*, 2010, **22**, 1060.
39 F. Sciortino, A. Giacometti and G. Pastore, *Phys. Chem. Chem. Phys.*, 2010, **12**, 11869.
40 Q. Chen, J. K. Whitmer, S. Jiang, S. C. Bae, E. Luijten and S. Granick, *Science*, 2011, **331**, 199.
41 R. Fantoni, A. Giacometti, F. Sciortino and G. Pastore, *Soft Matter*, 2011, **7**, 2419.
42 E. Zaccarelli, S. V. Buldyrev, E. La Nave, A. J. Moreno, I. Saika-Voivod, F. Sciortino and P. Tartaglia, *Phys. Rev. Lett.*, 2005, **94**, 218301.
43 E. Bianchi, J. Largo, P. Tartaglia, E. Zaccarelli and F. Sciortino, *Phys. Rev. Lett.*, 2006, **97**, 168301.
44 B. Ruzicka, E. Zaccarelli, L. Zulian, R. Angelini, M. Sztucki, A. Moussad, T. Narayanan and F. Sciortino, *Nat. Mater.*, 2011, **10**, 56.
45 G. Munaó, D. Costa and C. Caccamo, *J. Chem. Phys.*, 2009, **130**, 144504.
46 G. Munaó, D. Costa and C. Caccamo, *Chem. Phys. Lett.*, 2009, **470**, 240.
47 D. J. Tildesley and W. B. Streett, *Mol. Phys.*, 1980, **41**, 85.
48 M. P. Taylor and J. E. G. Lipson, *J. Chem. Phys.*, 1994, **110**, 518.
49 J. P. Hansen and I. R. McDonald, *Theory of Simple Liquids*, Academic Press, New York, 3rd edn, 2006.
50 C. Caccamo, *Phys. Rep.*, 1996, **274**, 1.
51 D. Chandler and H. C. Andersen, *J. Chem. Phys.*, 1972, **57**, 1930.
52 L. J. Lowden and D. Chandler, *J. Chem. Phys.*, 1974, **61**, 5228.
53 L. Lue and D. Blankschtein, *J. Chem. Phys.*, 1995, **102**, 5427.
54 A. Kovalenko and F. Hirata, *J. Theor. Comput. Chem.*, 2002, **1**, 381.
55 B. M. Pettitt and P. J. Rossky, *J. Chem. Phys.*, 1983, **78**, 7296.
56 B. Kvamme, *Phys. Chem. Chem. Phys.*, 2002, **4**, 942.
57 D. Costa, G. Munaò, F. Saija and C. Caccamo, *J. Chem. Phys.*, 2007, **127**, 224501.
58 L. Harnau, J.-P. Hansen and D. Costa, *Europhys. Lett.*, 2001, **53**, 729.
59 D. Costa, J.-P. Hansen and L. Harnau, *Mol. Phys.*, 2005, **103**, 1917.
60 J. P. Hansen and C. Pearson, *Mol. Phys.*, 2006, **104**, 3389.
61 P. G. Khalatur, L. V. Zherenkova and A. R. Khokhlov, *J. Phys. II*, 1997, **7**, 543.
62 W. Kung, P. González-Mozuelos and M. O. de la Cruz, *Soft Matter*, 2010, **6**, 331.
63 G. Munaó, D. Costa, F. Sciortino and C. Caccamo, *J. Chem. Phys.*, 2011, **134**, 194502.
64 M. Tripathy and K. S. Schweizer, *J. Phys. Chem. B*, 2013, **117**, 373.
65 P. Virnau and M. Müller, *J. Chem. Phys.*, 2004, **120**, 10925.
66 A. M. Ferrenberg and R. H. Swendsen, *Phys. Rev. Lett.*, 1989, **63**, 1195.
67 T. Morita and K. Hiroike, *Prog. Theor. Phys.*, 1960, **23**, 1003.
68 S. J. Singer and D. Chandler, *Mol. Phys.*, 1985, **55**, 621.
69 B. J. Schulz, K. Binder, M. Müller and D. P. Landau, *Phys. Rev. E*, 2003, **67**, 067102.
70 A. Stradner, H. Sedgwick, F. Cardinaux, W. C. K. Poon, S. U. Egelhaaf and P. Schurtenberger, *Nature*, 2004, **432**, 492.
71 Y. Liu, E. Fratini, P. Baglioni, W.-R. Chen and S.-H. Chen, *Phys. Rev. Lett.*, 2005, **95**, 118102.
72 F. Cardinaux, A. Stradner, P. Schurtenberger, F. Sciortino and E. Zaccarelli, *Europhys. Lett.*, 2007, **77**, 48004.
73 J. M. Bomont, J. L. Bretonnet and D. Costa, *J. Chem. Phys.*, 2010, **132**, 084506.
74 Y. Liu, L. Porcar, J. Chen, W.-R. Chen, P. Falus, A. Faraone, E. Fratini, K. Hong and P. Baglioni, *J. Phys. Chem. B*, 2011, **115**, 7238.
75 P. Falus, L. Porcar, E. Fratini, W.-R. Chen, A. Faraone, K. Hong, P. Baglioni and Y. Liu, *J. Phys.: Condens. Matter*, 2012, **24**, 064114.
76 N. H. March and M. P. Tosi, *Introduction to Liquid State Physics*, World Scientific Publishing, 2002.
77 P. T. Cummings, C. G. Gray and D. E. Sullivan, *J. Phys. A*, 1981, **14**, 1483.
78 D. Frenkel and B. Smit, *Understanding Molecular Simulations*, Academic, New York, 1996.